

Sensitivity of the East Asian Summer Monsoon Circulation and Precipitation to an Idealized Large-Scale Urban Expansion

Haiyan SHAO

*Key Laboratory of Meteorological Disaster of Ministry of Education, Nanjing University of
Information Science and Technology, Nanjing, China*

Jie SONG

Northern Illinois University, DeKalb, IL 60115, USA

and

Hongyun MA

*Key Laboratory of Meteorological Disaster of Ministry of Education, Nanjing University of
Information Science and Technology, Nanjing, China*

(Manuscript received 12 July 2012, in final form 21 December 2012)

Abstract

A numerical simulation was performed here using a regional climate model (RegCM3) at 60-km horizontal resolution to estimate the maximum impact of urbanization in East Asia on the summer monsoon precipitation in China. A new bulk urban parameterization was added into the land-surface scheme to capture the thermal, dynamic, and hydraulic effects of urban land cover. The 9-year simulation results showed that the large-scale change from natural-surface to high-density urban land cover induced an enhancement in the southwesterly wind speed in the early monsoon season across eastern China. In July and August, the enhanced southwesterlies moved to northern China, while a weakened southwesterly wind speed appeared south of the Yangtze River valley (YRV). Meanwhile, a large reduction in rainfall occurred in southern China with most reduction accounted for by convective precipitation reduction. This corresponded to the reduced water-vapor supply from the weakened southwesterlies in southern China, decreased convergence in the YRV, reduced convective instability in the lower troposphere, and lessened evapotranspiration from the impervious urban surface. Accompanied by the increased southwesterlies in the west and northwest of the urban region, a moderate increase in rainfall occurred in northern China. The changes in southwesterly wind speed and rainfall in southern China were more evident in the weak East Asian summer monsoon (EASM) years than in the strong ones. This underlines the impact of change in large-scale intensive urban land use on regional climate in the weak phase of the EASM. As fractional urban land cover was reduced, the changes in wind and precipitation were still shown but the spatial coverage and magnitude of these changes were reduced.

Keywords Urban land cover; East Asian summer monsoon; regional climate model; urban parameterization; precipitation

1. Introduction

The East Asian summer monsoon (EASM), driven by the temperature differences between the Asian continent and the Pacific Ocean, displays a distinct

Corresponding author: Jie Song, Department of Geography,
Northern Illinois University, DeKalb, IL 60115, USA.
E-mail: jsong@niu.edu
©2013, Meteorological Society of Japan

stepwise northward and northeastward seasonal progress (Ding and Chan 2005). During the summer monsoon season, water vapor originating from the South China Sea-western tropical Pacific region is advected by the southwesterly monsoon wind along the Meiyu-Baiu front. The onset of the summer monsoon is marked by a period of premonsoonal rain over South China in early May. Following the seasonal march, the summer monsoon shifts through a series of dry and rainy phases as the rain belt moves northward, beginning over Indochina and the South China Sea (May), to the Yangtze River valley and Japan (June), and finally to North China and Korea (July). The EASM ends in August when the rain belt moves back to South China (Wang 2006).

An apparent negative correlation is found between the strength of the EASM and summer (JJA) rainfall in the middle and lower reaches of the Yangtze River Valley (YRV) on the basis of the common definition of the EASM index (Li and Zeng 2005; Huang 2004). A strong EASM is characterized by a weak western Pacific subtropical pressure (WPSP), rapid northward advancement in the southerly flow, and water-vapor convergence located to the north of the YRV, all of which result in a dry summer over the YRV but a wet summer in northern China. During a weak EASM, the WPSP is strong and its western edge is located to the west of its climatic position. The westward expansion in the WPSP blocks the strong southerly flow from developing to the north of the YRV causing flood over the YRV but drought in northern China (Lu et al. 2007; Chen and Wu 1998).

As Wang (2006) pointed out, monsoons are a response of the coupled atmosphere–ocean–land system to annual variations in solar forcing. A large change in one of the components, such as land surface, may result in a noticeable response from the system. On the basis of a numerical study, Takata et al. (2009) and Yamashima et al. (2011) found that land use/cover change due to preindustrial cultivation had resulted in a decrease in monsoon rainfall over the Indian subcontinent and southeastern China and an associated weakening of the Asian summer monsoon circulation. The decrease in precipitation in southern China was contributed by the decrease in water-vapor flux convergence due to atmospheric circulation changes, while the decrease in precipitation in the Indian subcontinent was caused by a marked decrease in evapotranspiration.

Over recent decades, rapid urban development in East Asia, especially in the eastern part of China, has dramatically modified the thermal and dynamic

characteristics of the natural surface. Variations in urban surface characteristics are known to alter the local climate through modification of land-surface processes that influence the surface energy balance and boundary layer and lead to distinct urban climates. China is the largest country in Asia, and Chinese people make up one-fifth of the world's population. According to a land cover product derived from moderate-resolution imaging spectroradiometer (MODIS) data in 2007, the percentage urban fraction at 10-km resolution varies from less than 10% in suburban areas to greater than 60% in large metropolitan regions in East Asia. High urban fractions dominate east of 110°E, including Korea and Japan. Currently, over 50% of China's population lives in urban areas, and this proportion is predicted to grow beyond 77% by 2050 (United Nations 2011, 2012). It is expected that urban land cover will be an important landscape feature that cannot be overlooked, particularly for the EASM studies.

Effects of the urban heat island on regional temperatures and wind have been well studied and simulated. By using numerical simulation and observation, Zhang et al. (2009) showed that the upstream urbanization effect could cascade downwind and produce distinct meteorological consequences far from the city. Other evidence suggests that the effect of urban areas on the regional atmospheric environment goes beyond the urban heat island to encompass precipitation and convective processes (Shepherd 2005; Shepherd et al. 2010a). Regional-scale studies have shown that urban areas significantly enhance the intensity of storms and increase downwind rainfall (Changnon 1978; Shepherd et al. 2002). Using composite radar data, Ashley et al. (2011) and Bentley et al. (2010) demonstrated that urbanization augmented warm-season convection among a range of cities in the southeastern United States. With a similar method, Niyogi et al. (2011) showed that the intensity and structure of the thunderstorms were altered as they moved over Indianapolis, Indiana. Mitra et al. (2012) analyzed premonsoonal rainfall over a megalopolis in India and identified the possible association between urban land cover expansion and premonsoonal rainfall increase. Urbanization effects on heavy rainfall during the Indian summer monsoon were assessed by Kishtawal et al. (2010) with *in situ* and satellite-based precipitation. They found a significant increasing trend in the frequency of heavy rainfall over the urban regions of India during the monsoon season. Urban regions experience fewer occurrences of light rainfall and significantly higher occurrences of intense

precipitation compared to non-urban regions.

Previous observational studies have suggested that precipitation distribution could be modified by urban land cover. However, the impact of urbanization may be masked by large-scale climate variations because urban land cover in most parts of the world occupies a relatively small fraction in the global models' grid cells. Using empirical and remote-sensing data, Lamptey (2010) illustrated that urban land cover has the smallest impact on the surface energy budget compared with other land cover types at the global scale; however, the relative importance of the urban landscape increases as the fraction of urban land cover increases at the regional scale. Studies by Jin et al. (2005) showed that over large and dense urbanization regions, the size of urban regions increased dramatically to be comparable with global model grid cells. Jin et al. (2007) simulated and assessed the mechanisms and effects of the urban heat island using an offline single-column climate model coupled with a land surface model, in which data retrieved from satellite observations were used to represent the first-order urban effects. Their results suggest that human-activity-induced surface temperature hazards result in overlying atmosphere instability and enhanced convective rainfall.

To include urban effects in the land-surface model, Oleson et al. (2008) developed an urban parameterization module that is incorporated into the Community Land Model (CLM). Using the Community Climate System Model (CCSM4) coupled with the new urban module, Oleson (2012) examined how air temperatures in urban and rural areas might respond differently to changes in climate. This urban module is complex enough to include most of the important physical processes in urban climatology; however, its parameters are not easily obtained accurately. Jin and Shepherd (2005) suggested using satellite-based information to infer several key parameters required in the urban model, such as urban coverage, albedo, and LAI, but other required parameters, such as building height and roughness length, are still difficult to retrieve, which makes the understanding of urban properties and physical processes incomplete.

In this study, multi-year simulations of the effect of an idealized land use change are conducted using a regional climate model (RegCM3) from the Abdus Salam International Centre for Theoretical Physics. A new bulk urban parameterization is added to simulate the urban land cover effect on the atmosphere. The research objectives are to investigate (a) the maximum effect of large-scale urban land use on summer

monsoon circulation and precipitation in China, (b) the difference in the urbanization effect in strong and weak EASM circulation backgrounds, and (c) the difference in the urbanization effect as urban density decreases.

2. Model and experiment description

2.1 Model and urban parameterization

RegCM3 is a limited-area model whose dynamical component is similar to that of the hydrostatic version of the Pennsylvania State University (PSU)/National Center for Atmospheric Research (NCAR) mesoscale model (MM5). The model is a compressible, finite difference model with hydrostatic balance and terrain following vertical sigma-coordinates. The model considers the physical exchanges between the land surface, boundary layer, and free atmosphere through parameterizations of surface, boundary layer, and moist processes. The Biosphere-Atmosphere Transfer Scheme (BATS) is used to compute surface-atmosphere exchange fluxes (Dickinson et al. 1993), and a simplified explicit moisture scheme is included to consider resolvable scale precipitation. A number of cumulus schemes such as the Grell scheme (Grell 1993), MIT-Emanuel scheme (Emanuel 1991; Emanuel and Zivkovic-Rothman 1999), and modified Kuo scheme (Anthes 1977) are included in the model. The radiation scheme of the NCAR Community Climate Model (CCM3) is used in the RegCM3. The standard vertical resolution is 18 levels with about five levels within the planetary boundary layer. More detailed description is available in RegCM Version 3.1 User's Guide (Elguindi et al. 2007).

RegCM3 has been run over various regions at grid spacing ranging from 10 to 100 km and simulation periods from days to decades in order to study regional climate and seasonal predictability around the world (Pal et al. 2007). RegCM3 has also been shown to be a valid tool to simulate the Asian summer monsoon (Park et al. 2008). Using RegCM3, Sinha et al. (2012) examined the sensitivity of the Indian summer monsoon simulations to several cumulus parameterization schemes included in the RegCM3. They found that at 90-km resolution, the Grell scheme and Anthes-Kuo scheme (both with Arakawa and Schubert closure) performed comparatively better than other cumulus schemes in terms of seasonal mean rainfall and circulation simulations. The Grell scheme is especially better in bringing out upper-air circulation features. In this study, the Grell scheme in RegCM3 is used to investigate sensitivities of convective precipitation to extreme urban land cover scenarios during the EASM. The non-convective clouds and precipitation are

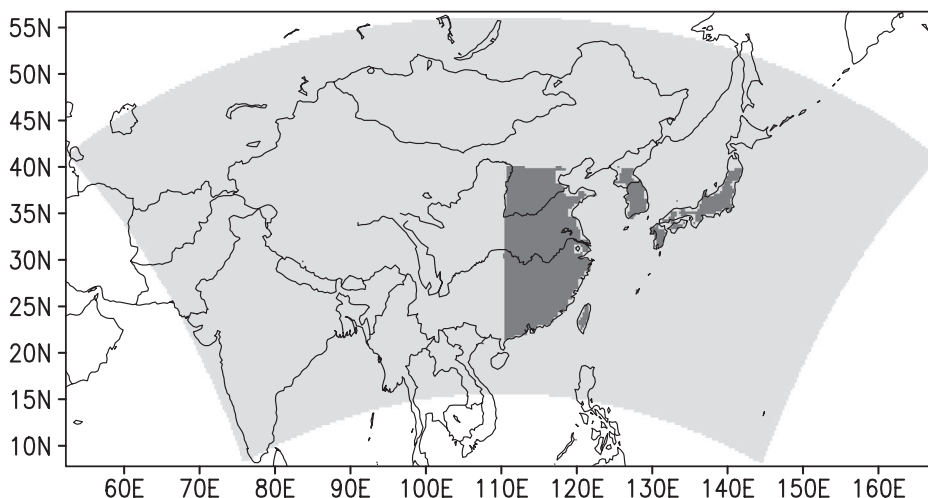


Fig. 1. Model simulation domain (light shade) and urban land cover setting (dark shade), with large-scale urbanization imposes 80% (high density 80%URB) or 20% (low density 20%URB) urban fraction between 20–40°N and east of 110°E including Korea and Japan. Huang River valley (HRV) is bounded by 35–43°N, east of 110–120°E and Yangtze River valley (YRV) is bounded by 25–35°N, 110–120°E.

resolved by the Subgrid Explicit Moisture Scheme by linking the average grid cell humidity to the cloud fraction and cloud water (Elguindi et al. 2007).

The modeling domain is set up with center at 35°N, 110°E (Fig. 1) and 76×144 pixels at 60-km horizontal resolution. There are 18 vertical levels and simulation time step is 150 s. Model physics for the planetary boundary layer, convective precipitation, and ocean flux parameterization are based on the Holtslag scheme, Grell scheme with Arakawa and Schubert closure assumption, and Zeng scheme, respectively (Elguindi et al. 2007). The lateral boundary condition is the linear relaxation technique involving 12 lateral grids. The land-surface model, BATS, plays the most important role in this land use change study.

There are three different (but overlapping) soil reservoirs in the BATS: upper layer, rooting zone, and total soil layer. In calculating soil water budgets, all three reservoirs gain the same amount of water from rainfall and lose the same amount from evaporation and surface runoff because these fluxes occur at the soil surface. Surface runoff considers that runoff occurs only over the fraction of grid-cells that are saturated, and it is parameterized on the basis of the net water applied to the surface and ratio of soil moisture to its saturation value at the top layer. Water loss from transpiration removes soil moisture from the rooting zone. Fluxes between soil layers affect each reservoir differently, and the runoff to the groundwater occurs only in the total soil reservoir. Soil moisture in each

soil reservoir is determined by solving conservation equations (Dickinson et al. 1993).

There are 20 types of natural land cover defined in BATS. Fractional vegetation cover varies over grid-cells from 10% in semi-desert to 90% in broadleaf evergreen forest while the rest of the grid-cell is covered by bare soil. The albedo of the bare soil is determined by soil color and soil moisture. Soil hydraulic characteristics depend on soil texture. Urban land cover is not considered in the original land cover type. There are two approaches currently available to simulate urban land cover in numerical models. An urban canopy module, which explicitly simulates two-dimensional, symmetrical street canyons with infinite length, has been applied in Weather Research and Forecasting (WRF) and CCSM4 (Chen et al. 2004; Oleson et al. 2008). A bulk-parameterization approach, which characterizes the physical properties of urban land cover in the land-surface model without explicitly resolving the detailed processes in the urban canopy, has been used to study the general dynamic, thermal, and hydraulic effects of urban land cover (Liu et al. 2004; Jin et al. 2007).

In this study, a bulk-parameterization approach is adopted and urban land cover is defined as type 21, which is composed of a vegetation fraction and urban fraction without bare soil. In China, urban landscapes are usually seen as a dense array of tall buildings surrounded by confined areas of brush, grass, and/or narrow rows of deciduous and evergreen trees. The

Table 1. Land-surface parameters for urban land use types.

Fractional vegetation cover	Vegetation type	Roughness length	Displacement height	Albedo	Soil texture	Heat capacity	Thermal conductivity
20%	forest/field mosaic	2 m	10 m	0.15	Sandy clay	$3 \times 10^6 \text{ J m}^{-3} \text{ K}^{-1}$	$3.24 \text{ W m}^{-1} \text{ K}^{-1}$

type of urban vegetation chosen for urban land cover type 21 is forest/field mosaic, which is a dominant type in a typical city scene based on remote-sensing classification (Gao et al. 2002). The vegetation fraction represents urban greenbelt; the urban fraction, which occupies the rest of the grid-cell area besides the urban vegetation, is covered by buildings and paved ground. Its parameters are chosen on the basis of a typical Chinese metropolitan environment to evaluate the first order effect of urban land cover (Table 1).

To emphasize the effect of urban land use in East Asia on the region's monsoon climate, the urban fraction is chosen as 80% with the vegetation fraction 20%. To simulate the effect on momentum and heat exchanges, the roughness length for the urban fraction is chosen to be 2 meters with displacement height at 10 meters (Gao and Bian 2004; Liu et al. 2009). To simulate the albedo reduction due to black pavement and "cavity effect" with multiple internal reflections resulting from the urban "canopy" geometry, a darker surface color is chosen for the urban fraction. The corresponding urban surface albedo typifies the observed albedo (0.15) in districts with mixed business and residential quarters in Beijing (Jiang et al. 2007) and agrees with the MODIS data shown in Jin et al. (2005).

The effect of a large urban heat reservoir on the atmosphere is simulated by imposing a relatively large heat capacity ($3 \times 10^6 \text{ J m}^{-3} \text{ K}^{-1}$) and thermal conductivity ($3.24 \text{ W m}^{-1} \text{ K}^{-1}$) on the basis of urban parameters used in Liu et al. (2004) and Chen et al. (2004). To simulate the effect of reduced evapotranspiration due to concrete and asphalt surfaces as well as drainage system, the hydraulic properties of the urban surface are assumed to be those of sandy clay to lower soil moisture availability. The above bulk urban parameterization scheme (Table 1) is blended into the land-surface scheme in BATS.

2.2 Experiment design

In China, the unevenness of population distribution and economic development has led to a great contrast between eastern and western China in urban density distribution. The highest density of urban networks is

concentrated in the mid-latitude between 20 and 40°N and east of longitude 110°E (Ji et al. 2001; Yang and Gan 2004). The three megacities, the Bohai Economic Rim in northern China, Yangtze River Delta, and Pearl River Delta in southern China, are all located close to the coast of China. To emphasize the collective effect of large-scale urban land use on the regional climate, urban land cover is expanded to occupy the land area in the eastern part of East Asia between 20 and 40°N and east of 110°E (Fig. 1), which includes eastern China, Korean peninsula, and Japan but excludes mountainous regions in the Qinghai-Tibetan Plateau to the west. Such a subcontinental-scale urban land cover change is an exaggerated reality and is noticeably different from mesoscale studies of a single urbanized region.

The RegCM3 was driven by 2.5° resolution National Center for Environmental Prediction (NCEP)/National Center for Atmospheric Research (NCAR) reanalysis data at a 6-h interval. Model simulations were performed during monsoon from April 25 to August 31 in the years 1993, 1994, 1997, 1998, 2000, 2003, 2004, 2005, and 2009, and the results were analyzed for June–July–August (JJA). These years were chosen to reflect the large variability observed in the EASM indices (Li and Zeng 2005; Huang 2004). A strong EASM occurred in 1994, 1997, and 2004, a normal EASM in 2000, 2005, and 2009, and a weak EASM in 1993, 1998, and 2003. A climate pattern of "wet-north and dry-south" in eastern China is associated with the strong EASM, whereas "dry-north and wet-south" is associated with the weak EASM.

In the control simulations (CTL), urban land cover was not considered, and the natural land surface was modeled by the default BATS scheme. In the urban simulations (80%URB), urban land parameters were blended into the BATS scheme, and the urban fractional cover was chosen as 80%. In addition, simulations with 20% urban fraction (20%URB) were performed in the 9 years in order to compare the urban effect under different urban intensification conditions.

3. Results

3.1 Model evaluation

A fundamental feature of a typical monsoon is

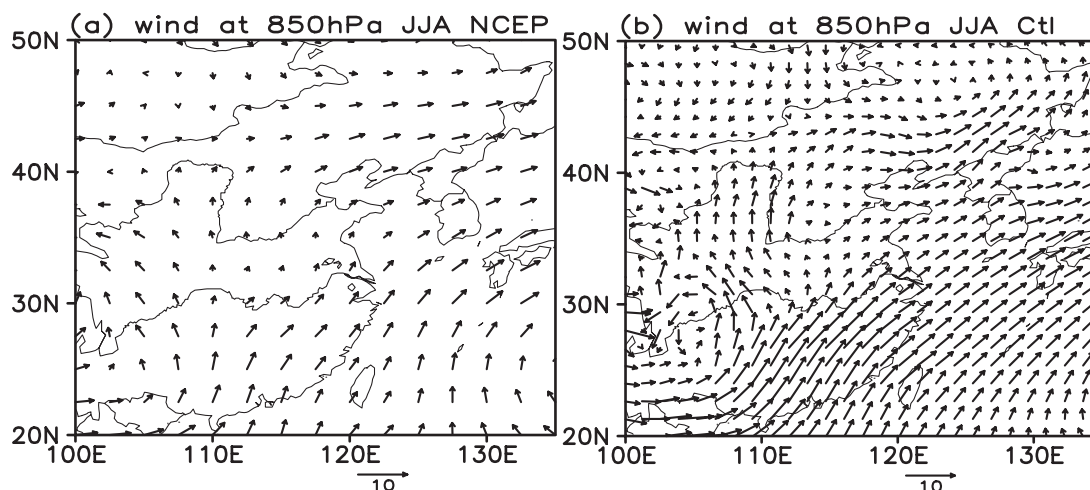


Fig. 2. Horizontal wind (m s^{-1}) at 850 hPa averaged in the 9 years during JJA. (a) NCEP reanalysis (at 2.5° resolution) and (b) Control-run simulation (at 60-km resolution).

seasonal variations in low-level wind. To evaluate the modeling ability for the EASM monsoon, modeled wind in the CTL was compared with the NCEP reanalysis data at the 850-hPa level (Fig. 2). Simulated wind in the control run shows that a strong southwesterly wind prevails in the Asian monsoon region during JJA, and the wind decreases toward the north with the largest convergence in the YRV near 30°N . The modeled wind field exhibits the typical monsoon wind patterns and agrees generally with the wind based on the NCEP reanalysis; however, the southwesterly wind is stronger and more westerly in southern China than that in the reanalysis data.

Modeled precipitation in the CTL was compared with data based on the Global Precipitation Climatology Project (GPCP) and observations interpolated from rain gauge data at 160 stations within China (Fig. 3). These observations show that rainfall is the largest in southern China, and it decreases northwestward in general; a moderate amount of precipitation falls in northeast China. Although the precipitation amount in the CTL is overestimated (Fig. 3c), the pattern of precipitation distribution agrees reasonably with the observations. In addition, model simulations implemented with an alternative MIT-Emanuel cumulus scheme at 60-km resolution were evaluated against these observations, and results from this scheme were not used for the urban land cover study owing to larger biases in simulated precipitation.

3.2 Urbanization experiments

Interactions between the land surface and atmos-

phere can be modified by large-scale urbanization through exchanges of momentum, heat, and water. Understanding the surface changes in surface drag, albedo, net radiation, and Bowen ratio is imperative for examining the urban effect on climate because of their thermal and dynamic processes in land-atmosphere interactions. Table 2 provides the comparison of these near-surface variables simulated in the summer monsoon season for the 9 years in the CTL and 80%URB runs. On average, surface drag stress, which is normalized by wind speed, is larger by $0.061 (\text{kg m}^{-2} \text{s}^{-1})$, surface albedo is lower by 0.038, and net radiation is higher by 38.8 W m^{-2} in 80%URB than those in the CTL. These changes in surface drag stress, albedo, and net radiation are consistent in all the simulation years and are the result of bulk urban parameterization (Table 1).

The Bowen ratio, defined as the ratio of sensible over latent heat flux, is higher by 1.1 on average over an urban land cover than that over a natural surface, indicating increased sensible heat flux and decreased latent heat flux. Higher Bowen ratio values simulated in 80%URB agree with the measurements by Coutts et al. (2007), who found that Bowen ratios at urban sites were greater than those at rural sites because of reduced evapotranspiration. The increases in net radiation and the Bowen ratio result in a 4.0°C increase in surface air temperature at 2 m and a 2.0 hPa decrease in sea-level pressure (SLP) on average (Table 2). The changes in the simulated Bowen ratio, surface temperature, and sea-level pressure due to urbanization are similar with the findings of Shem and

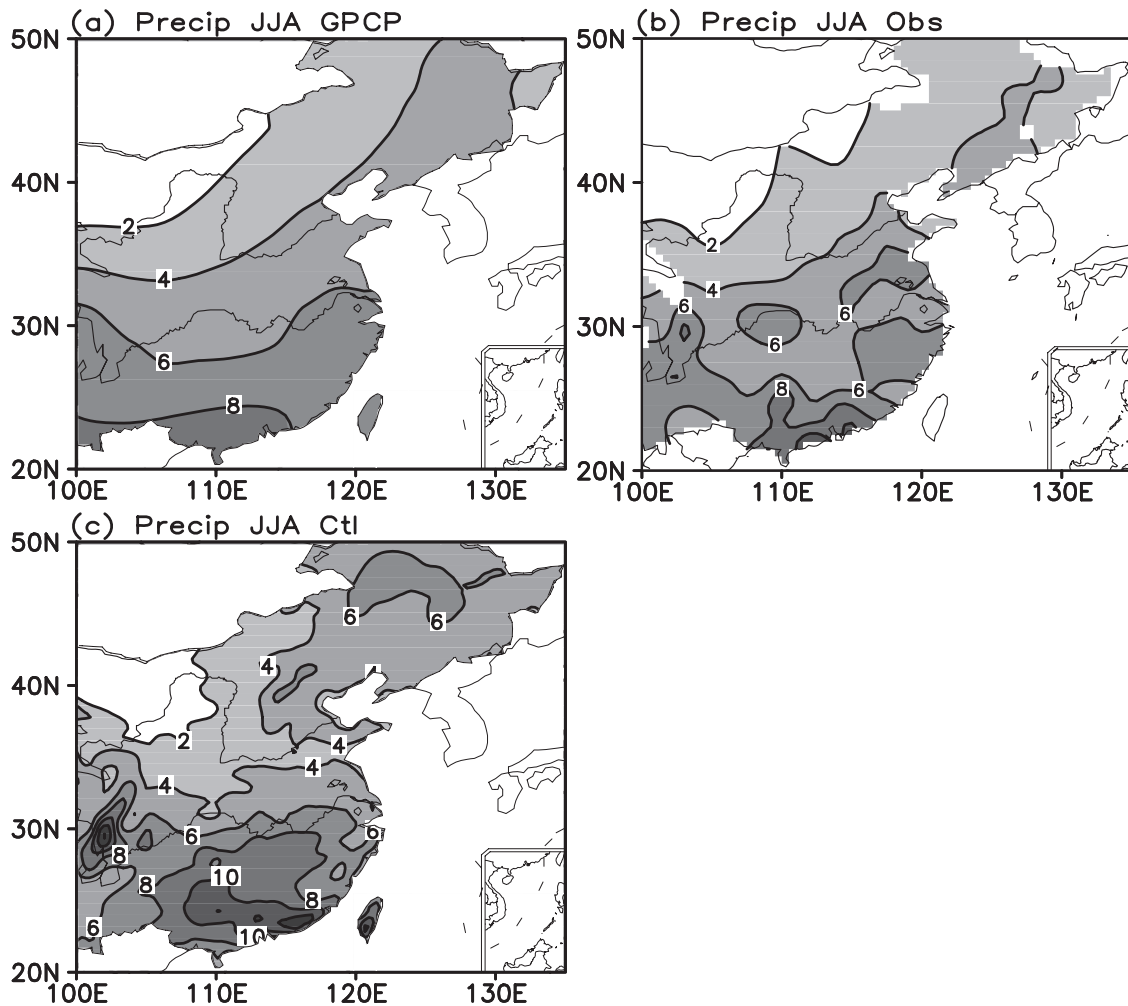


Fig. 3. Precipitation distribution (mm day^{-1}) averaged in the 9 years during JJA within China, (a) observation from Global Precipitation Climate Project (2.5° resolution), (b) observation from 160 stations in China, and (c) Control-run simulation.

Shepherd (2009) and Shepherd et al. (2010b).

a. Urban effect in general

The simulated EASM flow and precipitation with the inclusion of urban land cover were compared with the control runs in the nine EASM years to analyze the overall effect of urbanization on regional circulation and precipitation. The effect of urbanization on seasonal variations in low-level wind was examined at 850 hPa. The results are expected to clarify the changes in simulated rainfall.

When urban parameters are incorporated into the urban land type in eastern China, lower surface albedo and a drier surface produce a large heating source over the urban land cover (Tables 1 and 2). Geopotential

height at 850 hPa increases in the downwind urbanized region but decreases over the ocean on the east of China and over land on the west of the urbanized region (Fig. 4a). On the basis of the geostrophic wind principle, the higher geopotential height adds a clockwise wind rotation onto the southwesterly monsoon flow, resulting in decreased southwesterly flow to the south of the Yangtze River in eastern China but increased southwesterly flow to the west and northwest of the urbanized region (Fig. 4b). It is worth mentioning that in comparison with CTL runs, which do not include urban land cover (Fig. 2b), the decrease in the southwesterlies with the inclusion of urban land cover makes the modeled monsoon wind agree even better with the observation in southeastern China.

Table 2. Simulated surface drag stress, albedo, net radiation (Rn), Bowen ratio, 2-m temperature (T2m), and sea-level pressure (SLP) averaged over 25–40°N 110–118°E in strong (S), normal (N), and weak (W) EASM years during JJA.

Variable Average	Year		1993 (W)		1994 (S)		1997 (S)		1998 (W)		2000 (N)		2003 (W)		2004 (S)		2005 (N)		2009 (N)	
			Ctl	Urb	Ctl	Urb	Ctl	Urb	Ctl	Urb	Ctl	Urb	Ctl	Urb	Ctl	Urb	Ctl	Urb	Ctl	Urb
Drag ($\text{Kg m}^{-2} \text{s}^{-1}$)			0.025	0.082	0.025	0.088	0.025	0.083	0.026	0.079	0.025	0.087	0.025	0.086	0.024	0.085	0.024	0.089	0.024	0.091
albedo			0.170	0.125	0.170	0.135	0.170	0.132	0.170	0.127	0.171	0.134	0.169	0.133	0.171	0.134	0.171	0.136	0.171	0.138
Rn (W m^{-2})			232.9	264.2	250.7	287.9	247.4	280.7	233.7	262.9	257.0	313.5	241.1	278.9	263.0	304.4	256.8	288.5	257.5	308.2
Bowen ratio			0.189	0.739	0.248	1.603	0.244	1.088	0.202	0.761	0.269	1.868	0.200	1.168	0.247	1.452	0.234	1.31	0.224	1.827
T2m (K)			296.6	298.7	297.3	301.9	296.8	300.1	296.8	299.2	297.1	302.3	296.6	300.4	296.9	301.3	297.5	301.9	297.4	303.2
SLP (hPa)			1004.1	1002.9	1005.1	1002.7	1005.8	1004.2	1004.8	1003.6	1006.2	1003.6	1006.2	1004.6	1006.7	1004.3	1004.5	1002.6	1004.7	1001.8

Because of the urbanization effect, southwesterlies appear to be influenced differently to the east and west of 115°E on the basis of their JJA field (Fig. 4a). Temporal variations in urban influence on the meridional wind averaged for the 9 years over 110–115°E and 115–120°E are further examined in Figs. 4c and 4d, respectively. Over the 110–115°E region (Fig. 4c), it is shown that urbanization increases meridional wind in the early May across 20–45°N latitude, which indicates that the monsoon wind may start early in the season possibly because of a larger thermal contrast between land and ocean. This finding agrees with a recent research by Mitra et al. (2012), who documented the enhanced premonsoonal pattern due to land use change in a part of India. By late May and early June the increased meridional wind is confined to 25–30°N. The largest increase in meridional wind occurs in late June to early August, and it is positioned north of the YRV between 29–35°N. Meanwhile, a large decrease in meridional wind occurs to the south of the YRV.

As a result of the weakened southerly flow to the south of the YRV, water-vapor transport by the monsoon flow is weak and the moisture convergence near the YRV is greatly reduced in July and August. Over the 115–120°E region (Fig. 4d), an increase in the meridional flow between 20–45°N appears to be greater than its western counterpart during early monsoon. By late June, the increased meridional flow becomes weaker; it is shifted to the north of 35°N during July and August. Meanwhile, a remarkable decrease in the meridional flow south of the YRV occurs, which weakens the convergence of the monsoon circulation over the YRV.

In Asia, the precipitation amount and distribution during the EASM is vital to agriculture and human lives. Modeled large-scale modification of the land surface significantly decreases the precipitation to the south of the Huang River Valley (HRV) but increases the precipitation in northern China (Fig. 5a). These changes in precipitation are significant at 90% confidence level. Regions in southern China (23–28°N, 100–117°E) and YRV (29–34°N, 113–120°E), where precipitation is reduced the most (Fig. 5a), are examined in their corresponding areal averaged equivalent potential temperature profiles (Fig. 5b).

The result is that equivalent potential temperature is reduced in the lower troposphere but is increased above till 500 hPa owing to urban land cover. The decrease in the equivalent potential temperature appears to be caused by the large reduction in water-vapor content in the lower troposphere, even though the air temperature is increased over the urban land.

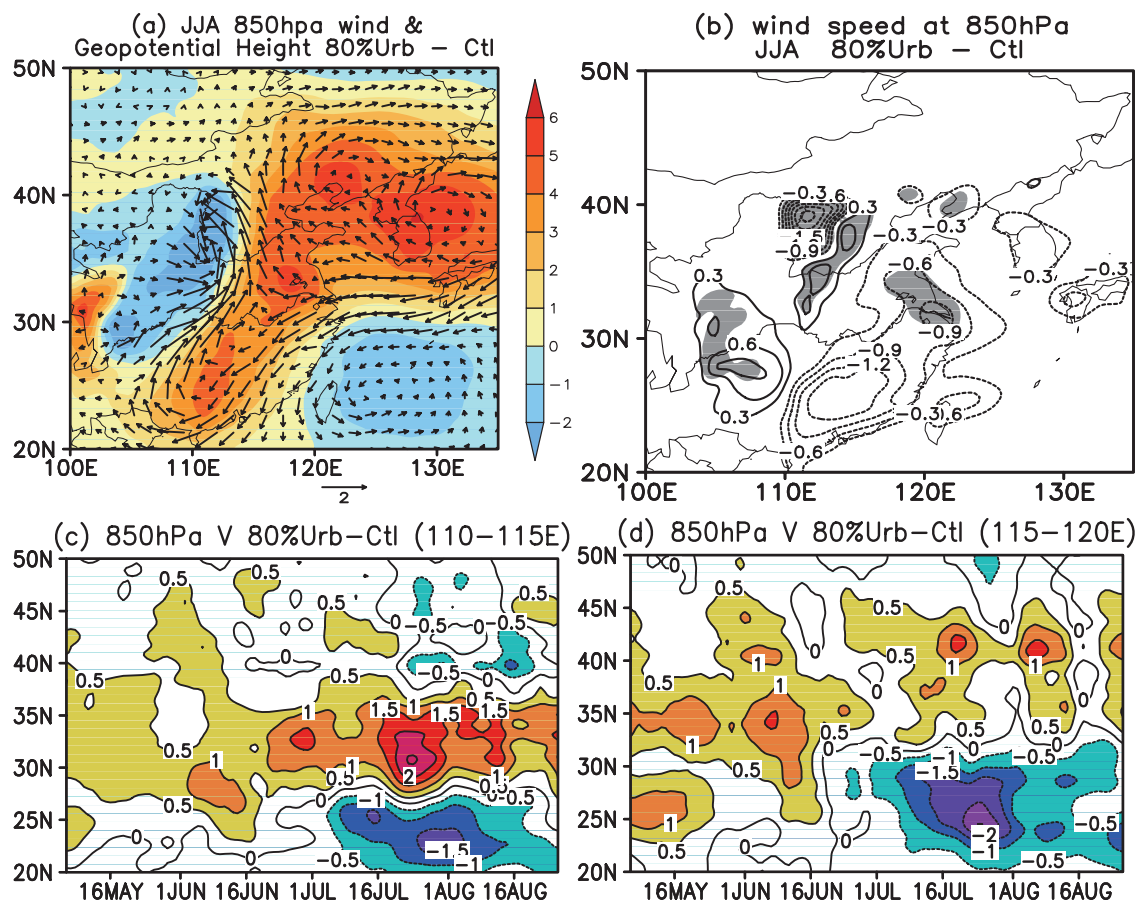


Fig. 4. Differences in simulated fields (80%URB minus CTL) averaged in the 9 years, (a) 850 hPa wind (m s^{-1}) and geopotential height (m), (b) 850 hPa wind speed (m s^{-1}) (the values in the shaded areas are significant at 90% t-test confidence level), and (c) and (d) latitude-time cross sections of 850 hPa meridional wind (m s^{-1}) averaged over 110–115°E and 115–120°E, respectively. All values in (c) and (d) are 11-day running means and differences larger than 0.5 m s^{-1} are colored.

These changes lead to a reduced potential instability below 800 and 700 hPa for southern China and YRV region, respectively, and increased potential instability above the corresponding levels but below 500 hPa. The reduced potential instability in the lower troposphere causes a large convective inhibition (CIN), which would reduce the chance of light convective rainfall. Because of the reduction in weak convection, convective available potential energy (CAPE) is accumulated continuously in the atmosphere. Once CIN is overcome by an episodic trigger, a large amount of CAPE needs to be released in the form of intensive precipitation. This result agrees with previous studies in that urban regions experience fewer occurrences of light rainfall but significantly higher occurrences of intense precipitation compared to non-urban regions.

Convective and non-convective precipitation are explicitly simulated by RegCM3 through the cumulus scheme and Subgrid Explicit Moisture Scheme, respectively. The latitude-time cross section of the simulated total precipitation show that changes due to urbanization occur mostly in July and August (Fig. 5c). Convective precipitation reduction accounts for most of the change south of the HRV, while a small increase in rainfall in northern China is due to an increase in non-convective rainfall (Fig. 5d).

In summary, three factors appear to contribute to overall rainfall reduction in the south of the HRV: (1) reduction in evapotranspiration in eastern China at 20–40°N due to a smaller vegetation cover fraction and a drier urban surface, (2) reduction in water-vapor transport due to the weakened southerly wind in

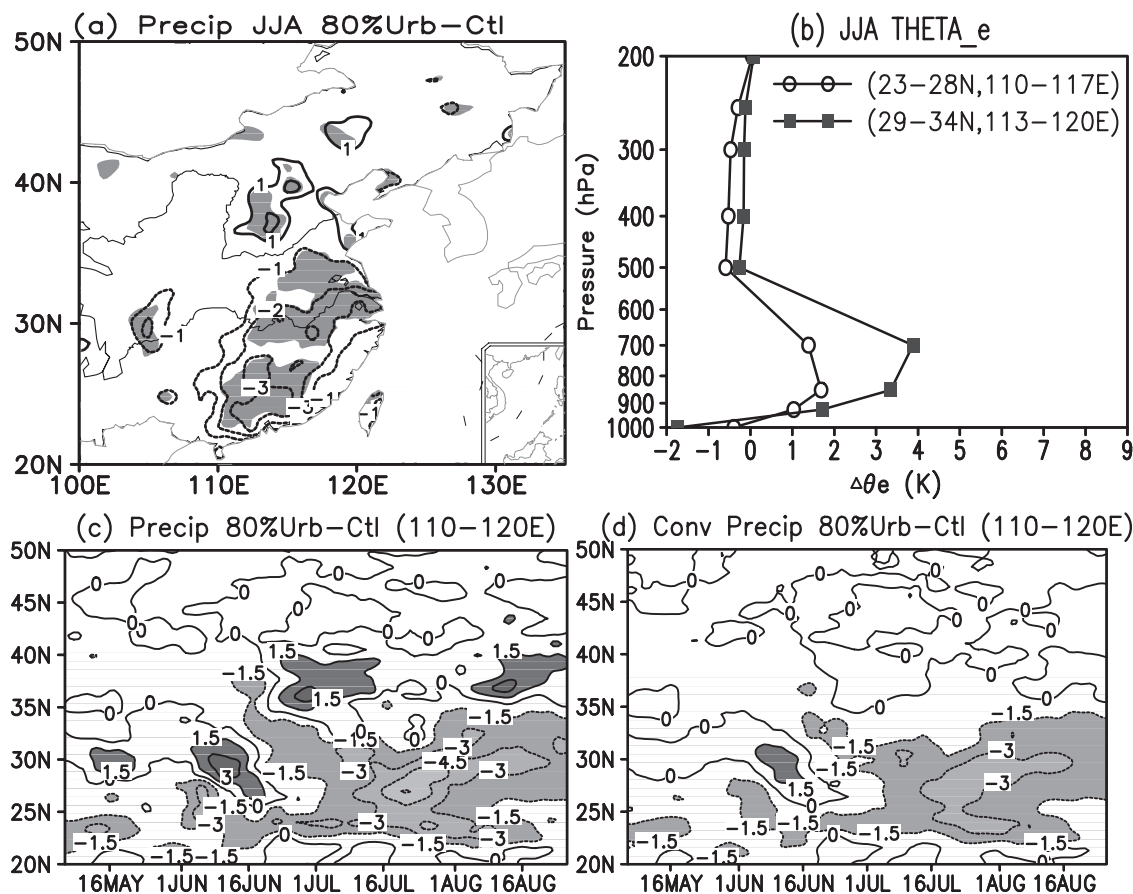


Fig. 5. Differences in simulated fields (80%URB minus CTL) averaged in the 9 years: (a) total precipitation difference (mm day^{-1}) (solid and dotted lines represent positive and negative values, respectively, and the values in the shaded areas are significant at 90% t-test confidence level), (b) vertical profile of simulated equivalent potential temperature difference averaged over 23–38°N, 110–117°E, and 29–34°N, 113–120°E, (c) latitude-time cross section of total precipitation difference (mm day^{-1}) with 11-day running mean averaged over 110–120°E (differences larger than 1.5 mm day^{-1} are shaded), and (d) same as (c) but for convective precipitation.

southeast China, and (3) reduction in convergence near the YRV. However, the slight increase in precipitation in northern China seems to be accompanied by convergence due to increased southwesterlies in the west and northwest of the urban region. Although the pattern of precipitation change in this study is similar to that over a single urban region (Changnon 1978; Shepherd et al. 2002), the subcontinental-scale collective urbanization effect not only impacts large-scale circulation (Fig. 4) but also evolves over time. It is worth mentioning that the precipitation reduction in southern China simulated with urban land cover reduces the overestimation biases in precipitation shown in the CTL (Fig. 3c).

b. Urban effect in strong and weak EASM years

Observations and research on interdecadal variations in the EASM have suggested a steady decline of East Asian monsoon wind in the recent three decades since the end of 1970s, which leads to less precipitation in northern China but more precipitation in southern China during summer (Xu et al. 2006; Wang 2001; Gong and Ho 2002). To find out whether the impact of urban land use is the same during strong and weak EASM circulation, the modeling results are analyzed for strong (1994, 1997, and 2004) and weak (1993, 1998, and 2003) EASM years. During the strong EASM, monsoon rainfall advanced furthest to the northernmost region in China but was nearly absent in southern China. On the other hand, during the weak

EASM, monsoon rainfall only reached the southern part of China; it caused floods in the YRV and wet summers in the Korean peninsula and Japan (Shen et al. 2001).

The control runs during JJA show that the 850 hPa geopotential gradient is weak, and the weak southerly wind prevails in both southern and northern China during the three strong EASM years (Fig. 6a), whereas the geopotential gradient is strong, but strong southwesterlies reside only in the south of the YRV during the three weak EASM years (Fig. 6b). The increases in the geopotential height in the north (strong EASM years) and northeast (weak EASM years) directions of the downwind urbanized region clearly indicate the strength of thermal advection at 850 hPa. Although changes in these fields in general are similar to those in the multi-year average (Fig. 4a), the effect of urban land cover on wind field appears to be greater during the weak EASM years than those during the strong EASM years in the south of the YRV where monsoon wind tends to be strong during weak monsoon years, but the effect seems weaker in northeast China during the weak EASM years (Figs. 6c and 6d).

Precipitation is reduced south of the Huang River valley (HRV) but is slightly increased in the north of it during the strong EASM years (Fig. 6e). Precipitation reduction occurs mostly to the south of the YRV during the weak EASM years, but an increase occurs in the HRV and the middle reaches of the YRV (Fig. 6f). The changes are more evident during the weak EASM years owing to larger changes in the wind speed and direction (Fig. 6b).

c. Effect with reduced urban intensification

Urban intensity can vary greatly from the central metropolitan to suburban regions. As the fractional urban land cover decreases away from the urban center, the fractional vegetation cover increases. To examine the effect of high versus low urban intensity on the EASM precipitation, the fractional urban cover was reduced from 80% to 20% in each urban grid cell in eastern China, and the urbanization effect at 20% fractional urban cover (20%URB) was simulated in the same 9 years (Fig. 7). The pattern of precipitation changes (precipitation reduction and increase in southern and northern China) in 20%URB can still be identified with the pattern found in 80%URB (Fig. 6). However, the magnitude and extent of the urbanization effect on wind field and precipitation are significantly reduced as the fractional urban cover decreases to 20%. The results concerning fractional coverage

changes are consistent with experiments conducted for the Houston area by Shepherd et al. (2010b). They used past, current, and future urban land cover in MM5 to evaluate sensitivity to land cover fraction and found that larger urban land cover produced the most significant and widespread changes in regional rainfall.

4. Summary and discussion

The impact of large-scale urbanization in East Asia on the EASM was simulated using RegCM3 with an urban parameterization scheme that included potential feedback to the atmosphere and hydrological cycle. The emphases considered were (1) large fraction of impervious surfaces and reduced urban vegetation cover that impact surface temperatures and hydrology, (2) decreased albedo (by 0.038) that influences the net radiation budget (by 38.8 W m^{-2}), and (3) large roughness length that increases surface drag stress (by $0.061 \text{ kg m}^{-2} \text{ s}^{-1}$).

The extreme urbanization model—expanded urban land cover in eastern China with 80% fractional urban cover—was chosen to emphasize the effect of urban land cover on the monsoon climate. Large-scale intensive urbanization enhanced the southwesterlies over eastern China early in the monsoon season owing to a larger thermal contrast between urbanized land and ocean. In mid-July and August, the enhanced southwesterlies were confined to northern China. In the meantime, reduced southwesterlies occurred in southern China, which decreased water-vapor transport there and reduced convergence over the Yangtze region. In addition, urbanization decreased evapotranspiration and reduced low-level atmospheric instability; this caused a reduction in convective rainfall in southern China and the southeast coast but a small increase in non-convective rainfall in northern China.

It is possible that the modeled variables were underestimated (such as surface albedo) or overestimated (such as surface latent heat flux) in the CTL because of the overestimation in southwesterly wind and precipitation. The changes in these variables due to the 80%URB or 20%URB are much larger than their biases in the CTL. Further, the results show that the inclusion of urban land cover reduces the biases of the CTL in the wind and precipitation simulation in southern China. The study tested the modeling setup at 30-km resolution and the results were very close to those at 60-km resolution, except for the added detail in spatial variation.

It was also noticed that changes in the southwester-

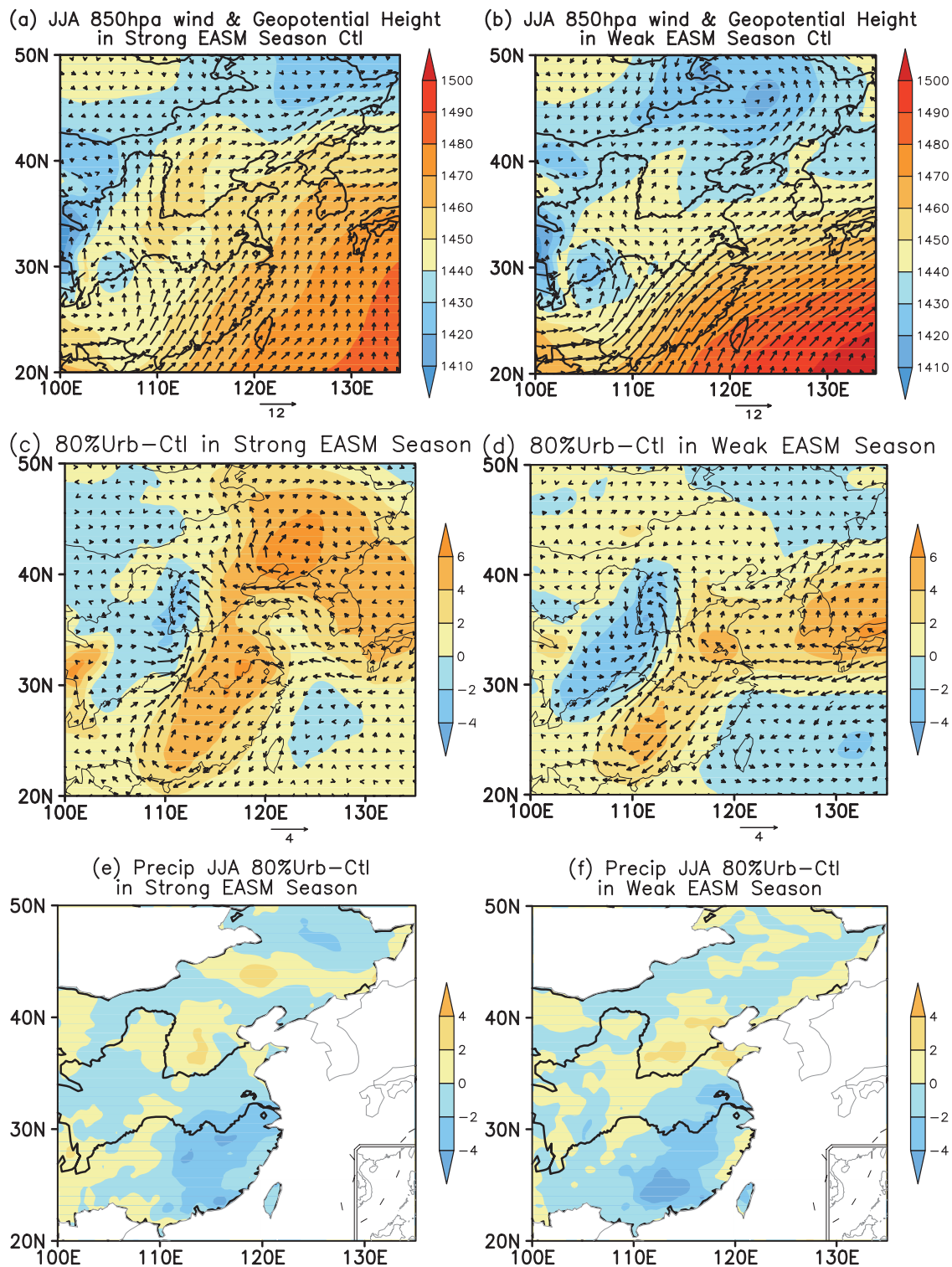


Fig. 6. Simulated JJA 850 hPa wind (m s^{-1}) and geopotential height (m) in CTL (upper panel), their corresponding differences: 80%URB-CTL (middle panel) and precipitation differences (mm day^{-1}): 80%URB-CTL (lower panel), averaged in three strong (left panel) and three weak (right panel) EASM years.

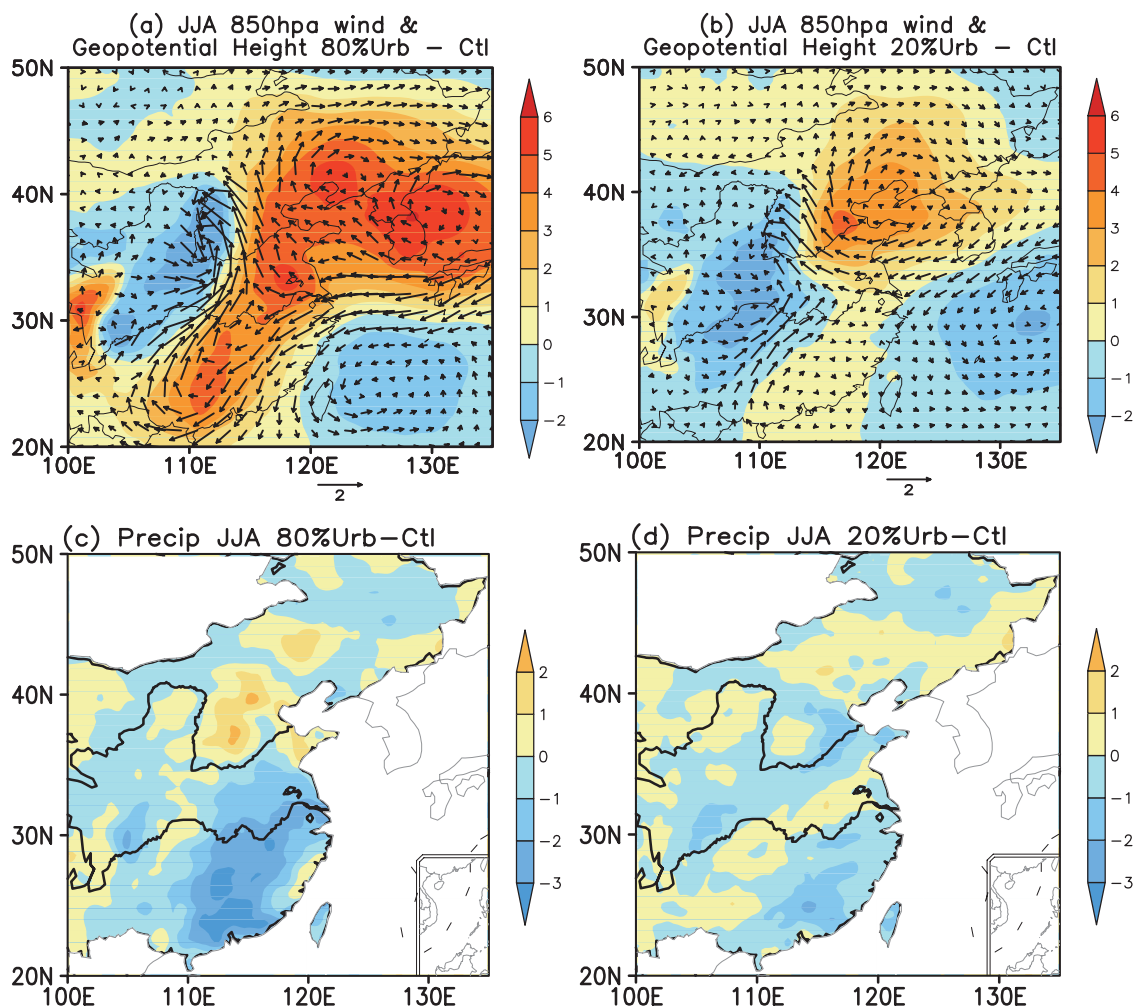


Fig. 7. Simulated 9-year JJA 850 hPa wind (m s^{-1}) and geopotential height (m) differences (upper panel) and precipitation difference (mm day^{-1}) (lower panel) between 80%URB-CTL (left panel) and 20%URB-CTL (right panel).

lies and precipitation due to urbanization were more evident during the weak EASM years, which suggests that impact of urban land use on the regional climate may be larger in a weak monsoon environment. As the fractional urban cover is reduced to 20%, the effects of urbanization can still be recognized, even though their extent and magnitude are greatly reduced.

The results of the sensitivity test indicate the importance of urban land cover effects in the East Asian monsoon as urbanization continues to intensify in eastern China. Although anthropogenic heating is not explicitly specified in the current study, the effect of thermal heating near the surface has been modeled by the overall increase in sensible heat flux due to the increase in net radiation and decrease in latent heat flux

with increased Bowen ratio (Table 2).

Finally, the simulated effects of urban land cover on wind and precipitation in East Asia seem to be opposite to the observed weakening of the EASM since the end of 1970s (Xu et al. 2006). This suggests that changes in land cover due to urbanization may not be an explanation for the weakening of the EASM. Increased aerosol loads associated with East Asian urbanization also would have effects on insolation and cloud microphysics. This is a possible missing piece in the puzzle related to the weakening of the EASM. Further research will incorporate the effect of atmospheric aerosols in conjunction with the urban canopy module to accurately account the effect of urbanization on the EASM climate.

Acknowledgements

This project is funded by the National Basic Research Program of China (973 Program 2010CB428505), the Priority Academic Program Development of Jiangsu Higher Education Institutions (PAPD), and the Jiangsu Meteorological Bureau (KM201102). We thank John Hudson at the Northwestern University for his careful editing.

References

- Anthes, R., 1977: A cumulus parameterization scheme utilizing a one-dimensional cloud model. *Mon. Wea. Rev.*, **105**, 270–286.
- Ashley W. S., M. L. Bentley, and J. A. Stallins, 2011: Urban-induced thunderstorm modification in the Southeast United States. *Climatic Change*, **113**, 481–498, doi: 10.1007/s10584-011-0324-1.
- Bentley, M. L., W. S. Ashley, and J. A. Stallins, 2010: Climatological radar delineation of urban convection for Atlanta, Georgia. *Int. J. Climatol.*, **30**, 1589–1594, doi: 10.1002/joc.2020.
- Chang, C.-P., Y.-Sh. Zhang, and T. Li, 2000: Interannual and Interdecadal Variations of the East Asian Summer Monsoon and Tropical Pacific SSTs. Part I: Roles of the Subtropical Ridge. *J. Climate*, **13**, 4310–4325.
- Chen, F., Y.-B. Liu, H. Kusaka, M. Tewari, J.-W. Bao, Ch.-F. Lo, and K.-H. Lau, 2004: Challenge of forecasting urban weather with NWP models, WRF/MM5 Joint Workshop 2004, NCAR, available online at <http://www.mmm.ucar.edu/mm5/workshop/ws04/Session1/Chen.Fei.pdf>.
- Chen, L.-T., and R.-G. Wu, 1998: Relationship between summer rainbelt patterns in the Eastern China and 500 hPa circulation anomalies over the Northern Hemisphere. *Sci. Atmos. Sinica*, **22**, 849–857.
- Coutts, A. M., J. Beringer, and N. J. Tapper, 2007: Impact of increasing urban density on local climate: Spatial and temporal variations in the surface energy balance in Melbourne, Australia. *J. Appl. Meteor. Climatol.*, **46**, 477–493.
- Dickinson R. E., H. A. Sellers, and P. J. Kennedy, 1993: *Biosphere-Atmosphere Transfer Scheme (BATS) version 1e as coupled to the NCAR Community Climate Model*. NCAR Technical Note, NCAR/TN-387 + STR, 72 pp.
- Ding, Y. and J.-C. L. Chan, 2005: The East Asian summer monsoon: an overview. *Meteorol. Atmos. Phys.*, **89**, 117–142.
- Elguindi, N., B. Xunqiang, F. Giorgi, B. Nagarajan, J. Pal, F. Solmon, S. Rauscher, and A. Zakey, 2007: RegCM version 3.1 user's guide. Abdus Salam International Centre For Theoretical Physics, 57 pp.
- Emanuel, K. A., 1991: A scheme for representing cumulus convection in large-scale models, *J. Atmos. Sci.*, **48**, 2313–2335.
- Emanuel, K. A., and M. Živković-Rothman, 1999: Development and evaluation of a convection scheme for use in climate models. *J. Atmos. Sci.*, **56**, 1766–1782.
- Gao, J., Y.-Ch. Song, and Q.-F. Zhang, 2002: Analysis on the characteristics of urban vegetation and is mapping based on remote sensing and geographic information system. *Acta Phytoecologica Sinica*, **26**, 1–9 (in Chinese).
- Gao Zh.-Q., and L.-G. Bian, 2004: Estimation of aerodynamic roughness length and displacement height of an urban surface from single-level sonic anemometer data. *Aust. Meteor. Mag.*, **53**, 21–28.
- Gong, D., and C. Ho, 2002: Shift in the summer rainfall over the Yangtze River valley in the late 1970s. *Geophys. Res. Lett.*, **29**, 1436, doi:10.1029/2001GL014523.
- Grell, G., 1993: Prognostic evaluation of assumptions used by cumulus parameterizations. *Mon. Wea. Rev.*, **121**, 764–787.
- Huang, G., 2004: An index measuring the interannual variation of the East Asian Summer Monsoon-The EAP index. *Adv. Atmos. Sci.*, **21**, 41–52.
- Ji, C.-Y., Q.-H. Liu, D.-F. Sun, Sh. Wang, P. Lin, and X.-W. Li, 2001: Monitoring urban expansion with remote sensing in China. *Int. J. Remote Sens.*, **22**, 1441–1455.
- Jiang, X.-Y., Ch.-L. Zhang, H. Gao, and Sh.-G. Miao, 2007: Impact of urban albedo change on urban heat island in Beijing-A case study. *Acta Meteor. Sinica*, **65**, 301–307 (in Chinese).
- Jin, M., R. E. Dickinson, and D. Zhang, 2005: The footprint of urban areas on global climate as characterized by MODIS. *J. Climate*, **18**, 1551–1565.
- Jin, M., and J. M. Shepherd, 2005: Inclusion of urban landscape in a climate model-how can satellite data help? *Bull. Amer. Meteor. Soc.*, **86**, 681–689.
- Jin, M., J. M. Shepherd, and C. Peters-Lidard, 2007: Development of a parameterization for simulating the urban temperature hazard using satellite observations in climate model. *Nat. Hazards*, **43**, 257–271, doi: 10.1007/s11069-007-9117-2.
- Kishtawal, C. M., D. Niyogi, M. Tewari, R. A. Pielke, and J. M. Shepherd, 2010: Urbanization signature in the observed heavy rainfall climatology over India. *Int. J. Climatol.*, **30**, 1908–1916, doi:10.1002/joc.2044.
- Lamptey, B., 2010: An analytical framework for estimating the urban effect on climate. *Int. J. Climatol.*, **30**, 72–88, doi:10.1002/joc.1873.
- Li, J., and Q. Zeng, 2005: A new monsoon index, its interannual variability and relation with monsoon precipitation. *Climatic and Environmental. Research.*, **10**, 351–365.
- Liu, G., J. Sun, and W. Jiang, 2009: Observational verification of urban surface roughness parameters derived from morphological models. *Meteor. Appl.*, **16**, 205–213, doi: 10.1002/met.109.
- Liu, Y., F. Chen, T. Warner, S. Swerdlin, J. Bowers, and S. Halvorson, 2004: Improvements to surface flux computations in a non-local-mixing PBL scheme, and

- refinements on urban processes in the Noah land-surface model with the NCAR/ATEC real-time FDDA and forecast system. 20th Conference on Weather Analysis and Forecasting/16th Conference on Numerical Weather Prediction. 11–15 January, 2004, Seattle, Washington.
- Lu, J.-M., Q.-Y. Zhang, Sh.-Y. Tao, and J.-H. Ju, 2007: Contrast analysis on atmospheric circulation and heat source anomalies in strong and weak years of East Asian Summer Monsoon. *J. Appl. Meteor. Sci.*, **18**, 442–451.
- Mitra, C., M. Shepherd, and T. Jordan, 2012: On the relationship between the pre-monsoonal rainfall climatology and urban land cover dynamics in Kolkata city, India. *Int. J. Climatol.*, **32**, 1443–1454.
- Niyogi, D., P. Patrick, L. Ming, S. P. Arya, C. M. Kishtawal, M. Shepherd, F. Chen, and B. Wolfe, 2011: Urban Modification of Thunderstorms: An Observational Storm Climatology and Model Case Study for the Indianapolis Urban Region. *J. Appl. Meteor. Climatol.*, **50**, 1129–1144, doi:10.1175/2010JAMC1836.1.
- Oleson K., 2012: Contrasts between urban and rural climate in CCSM4 CMIP5 climate change scenarios. *J. Climate*, **25**, 1390–412.
- Oleson K., G. B. Bonan, J. Feddema, M. Vertenstein, and C. S. B. Grimmond, 2008: An urban parameterization for a global climate model. Part I: Formulation and evaluation for two cities. *J. Appl. Meteor. Climatol.*, **47**, 1038–1060.
- Pal, J. S., and Coauthors, 2007: Regional climate modeling for the developing world: The ICTP RegCM3 and RegCNET. *Bull. Amer. Meteor. Soc.*, **88**, 1395–1409.
- Park, E.-H., S.-Y. Hong, and H.-S. Kang, 2008: Characteristics of an East-Asian summer monsoon climatology simulated by the RegCM3. *Meteor. Atmos. Phys.*, **100**, 139–158.
- Shem, W., and J. M. Shepherd, 2009: On the impact of urbanization on summertime thunderstorm in Atlanta: two numerical model case studies. *Atmo. Res.*, **92**, 172–189.
- Shen, X.-Sh., M. Kimoto, A. Sumi, A. Numaguti, and J. Matsumoto, 2001: Simulation of the 1998 East Asian Summer Monsoon by the CCSR/NIES AGCM. *J. Meteor. Soc. Japan*, **79**, 741–757.
- Shepherd, J. M., H. Pierce, and A. J. Negri, 2002: Rainfall modification by major urban areas: Observations from spaceborne rain radar on the TRMM satellite. *J. Appl. Meteor.*, **41**, 689–701.
- Shepherd, J. M., 2005: A review of current investigations of urban induced rainfall and recommendations for the future. *Earth Interact.*, **9**, 1–27.
- Shepherd, J. M., J. A. Stallins, M. Jin, and T. L. Mote, 2010a: Urbanization: Impacts on clouds, precipitation, and lightning. *Urban Ecological Ecosystems*, Peterson, J., and A. Volder (eds.), American Society of Agronomy-Crop Science Society of America-Soil Science Society of America: 354 pp.
- Shepherd, J. M., M. Carter, M. Manyin, D. Messen, and S. Burian, 2010b: The impact of urbanization on current and future coastal precipitation: a case study for Houston. *Environment and Planning. B: Planning and Design*, **37**, 284–304, doi:10.1068/b34102t.
- Sinha, P., U. C. Mohanty, S. C. Kar, S. K. Dash, and S. Kumari, 2012: Sensitivity of the GCM driven summer monsoon simulations to cumulus parameterization schemes in nested RegCM3. *Theor. Appl. Climatol.*, **112**, 285–306, doi:10.1007/s00704-012-0728-5.
- Takata, K., K. Saito, and T. Yasunari, 2009: Changes in the Asian monsoon climate during 1700–1850 induced by preindustrial cultivation. *Proc. Natl. Acad. Sci. USA*, **106**, 9586–9589.
- United Nations, Department of Economic and Social Affairs, Population Division, 2011: *World Population Prospects: The 2010 Revision*. New York, United Nations.
- United Nations, Department of Economic and Social Affairs, Population Division, 2012: *World Urbanization Prospects: The 2011 Revision*. New York, United Nations.
- Wang, B., 2006: *The Asian Monsoon*. Springer, 836 pp.
- Wang, H., 2001: The weakening of Asian monsoon circulation after the end of 1970s. *Adv. Atmos. Sci.*, **18**, 376–386, doi:10.1007/BF02919316.
- Xu, M., C.-P. Chang, C. Fu, Y. Qi, A. Robock, D. Robinson, and H. Zhang, 2006: Steady decline of east Asian monsoon wind, 1969–2000: Evidence from direct ground measurements of wind speed. *J. Geophys. Res.*, **111**, D24111.
- Yamashita R., K. Takata, J. Matsumoto, and T. Yasunari, 2011: Numerical study of the impacts of land use/cover changes between 1700 and 1850 on the seasonal hydroclimate in monsoon Asia. *J. Meteor. Soc. Japan*, **89**, 291–298.
- Yang, G. and G.-H. Gan, 2004: Spatial characteristic and its change of urban system in China. *Geo-Information Science*, **6**, 12–18.
- Zhang, D. L., Y. X. Shou, and R. R. Dickerson, 2009: Upstream urbanization exacerbates urban heat island effects. *Geophys. Res. Lett.*, **36**, L24401, doi:10.1029/2009GL041082.